*Advanced Materials Research* *Online: 2014-08-11*
*ISSN: 1662-8985, Vol. 996, pp 878-883*
*doi:10.4028/www.scientific.net/AMR.996.878*


# Time-resolved X-ray stress analysis in multilayered thin films during continuous loading: use of 2D remote detection

Guillou.R[1, a,*], Renault.PO[1, b], Le Bourhis.E[1 ,c], Goudeau.P[1, d], Godard.P[1, e], Geandier.G[2, f], Faurie.D[3, g,] Thiaudière.D[4, h], Mocuta.C[4, i]

[1] Institut PPRIME-CNRS/Université de Poitiers/ENSMA, Futuroscope France

[2] IJL/SI2M -CNRS Université de Lorraine, Nancy, France

[3] LSPM-CNRS Université Paris 13, Villetaneuse, France

[4] Synchrotron SOLEIL, Gif sur Yvette, France

[a] raphaelle.guillou@univ-poitiers.fr, [b] pierre.olivier.renault@univ-poitiers.fr,
[c] eric.le.bourhis@univ-poitiers.fr, [d] philippe.goudeau@univ-poitiers.fr,
[e] pierre.godard@univ-poitiers.fr, [f] guillaume.geandier@univ-lorraine.fr,
[g] faurie@univ-paris13.fr, [h] thiaudiere@synchrotron-soleil.fr,
[i] cristian.mocuta@synchrotron-soleil.fr

**Keywords:** nanostructured thin films, in-situ biaxial tension test, X-ray diffraction, Digital image correlation, strain measurements, stress analysis, 2D detector

## Abstract

Synchrotron X-ray diffraction is a powerful tool to analyse the mechanical behavior of multiphase materials due to its selectivity. Simultaneous stress analysis of both phases of a W/Cu thin multilayer has been performed during a continuous biaxial loading on DiffAbs beamline at SOLEIL synchrotron (France). The use of a 2D detector with a large sample-detector distance is shown to give relatively accurate applied stress analysis even if only a small part of the usual ψ range of the $\sin^2\psi$ method is considered. The results show the failure of the thin film multilayer while the W components are still under a strong compressive stress state of -3 GPa. It is concluded that the mechanical behavior is in fact mainly governed by the residual stress state.

## Introduction

In composite materials, measurements of separate diffraction peaks allow to investigate the mechanical behavior of each phase independently. In many situations due to the internal stresses, it is the ability of the composite to bear a large external load [1]. The residual stress state of thin films elaborated by physical vapor deposition technique can be of several GPa [2]. Moreover, the mechanical behavior of nanocrystalline material can be quite different from their coarse-grain counterpart [3]. In this study, the material is a composite at two levels: it is a metallic thin film deposited onto a polymeric substrate, and the thin film is composed of sublayers of W and Cu which are in the nanometer range. Sublayers' response has been simultaneously monitored using a 2D detector. In order to achieve accurate stress analysis, the 2D detector is located at relatively large distance from the sample to increase angle resolution. Analysis of experimental data allows studying the interactions between the film and the polymer substrate and between the two phases of the thin film itself during continuous equi-biaxial loading.

## Experiment set up

A biaxial tensile device [4] installed on the DiffAbs beamline at the synchrotron SOLEIL (Figure 1a) was used to test W/Cu thin films deposited by ion beam sputtering on polyimide cruciform substrates. The nanocomposite multilayer is composed of 7 periods of 24 nm (6 nm of W and 18 nm of Cu) thin films. The uncoated side of the substrate was spray-painting with a speckle pattern

in order to measure the applied strains with Digital image correlation (DIC) technique [5] in a central area of the cruciform substrate where the applied strains is uniform. Digital images of the specimen surface were captured with an optical camera fixed under the tensile device [6]. The mechanical responses of the two phases of the thin film were simultaneously monitored using X-Ray diffraction (XRD). The experiment was performed at synchrotron facility because of the small diffracting volume (polycrystalline film thickness of 150 nm) combined with the nanometric size of the grains yielding very broad and low-intensity diffraction peaks. We used a 0.3x0.3 mm² beam size and photon energy of 8.8 keV. This energy is below the Copper K-edge to minimize the background due to the fluorescence emission of this element. The detector was mounted on the detector arm of a six-circle goniometer with a relatively large sample to detector distance of 420 mm. This distance was chosen in order to optimize the resolution of applied stress analysis. Indeed small 2θ angles (low order reflections) have been monitored because of the very small diffracting volume (very thin films).

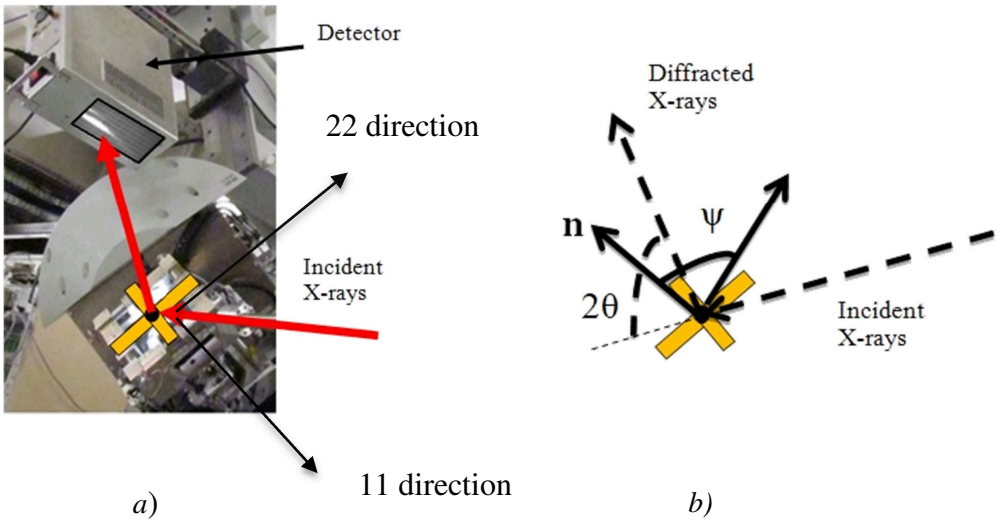


Figure 1 : a) Biaxial tensile device set on the goniometer of the DiffAbs beamline at the synchrotron SOLEIL. The optical microscope is located under the machine for macrostrain measurements at the center of the cruciform specimen. A remote two-dimensional XPAD detector is used to collect the X-ray diffraction patterns. b) Schematic representation of the experimental configuration: 2θ is the scattering angle (33-47° range) and ψ is the declination angle between the diffraction vector and the normal to the film surface **n** (64°-53° range).

2D detector (XPAD 3.2) has been chosen for its fast acquisition time and its two-dimensional geometry [7-8]. Data images were recorded every 18 seconds during a continuous equi-biaxial loading procedure. An initial equi-biaxial loading of 19 N was applied for the installation of the specimen on the biaxial tensile device, in order to avoid sample drift during deformation. An equi-biaxial test ranging from 19 to 160 N was performed. Forces applied along the two perpendicular axes and principal in-plane strains (macroscopic in-plane strains at the center of the cruciform substrate) obtained by DIC technique are shown in Figure 2. Interestingly, the two perpendicular axes (named 11 and 22) of the cruciform substrate have the same loading rate which decreases slightly during the test while the in-plane strain rates at the center of the cruciform shape substrate are significantly different and approximately constant. Linear fits lead to about $5.5\text{x}10^{-6}$ $s^{-1}$ for the 22 direction and $3.8\text{x}10^{-6}$ $s^{-1}$ for the 11 direction. These experimental measurements demonstrate the in-plane elastic anisotropy of the 125 µm-thick polyimide Kapton® films. X-Ray measurements were performed only along the 22 direction of the cruciform specimen (Figure 1).

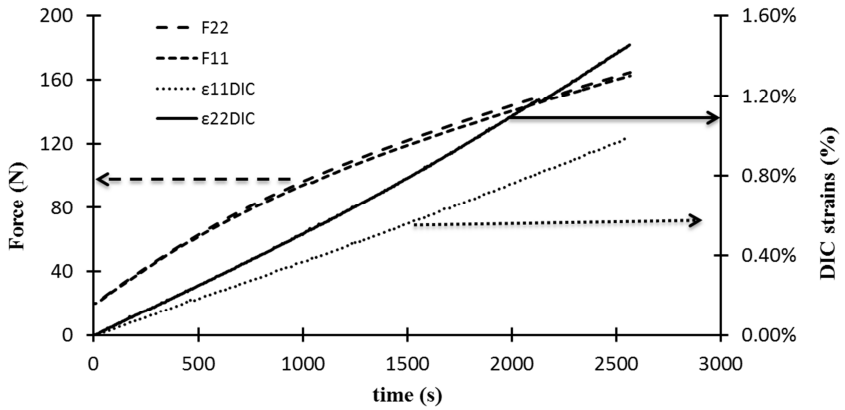


Figure 2: Evolution of the applied loads and principal in-plane strains (measured by Digital Image Correlation) at the center of the cruciform shape substrate as a function of time.

**Sin²ψ segments: extraction and analysis**

In the raw data image (Figure 3a), Debye-Scherrer rings for copper and tungsten can be observed. The first ring corresponds to the (110) reflection of W sublayers and the second to the (111) reflection of Cu sublayers. As W and Cu have respectively (110) and (111) fiber texture, the biaxial tensile device has been inclined at an angle ψ of 65° in order to monitor simultaneously Bragg peak shifts of the two phases of the multilayer thin films with a good accuracy. An integration procedure was used to get the classical pattern from which the Bragg peak positions are obtained by a fitting procedure (symmetric Pearson VII functions with linear background) (Figure 3b).

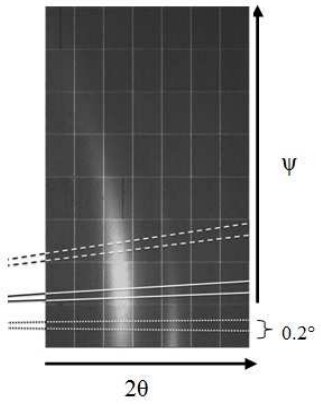


a)

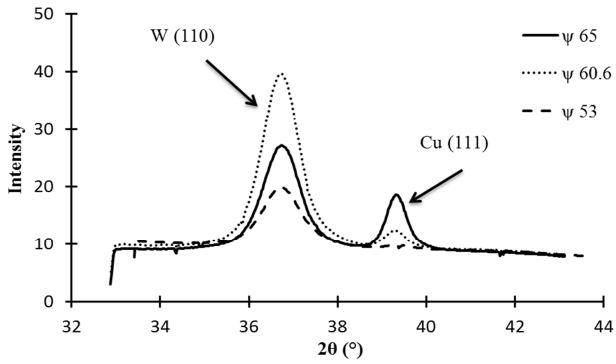


b)

Figure 3 : a) 2D diffraction pattern recorded by 2D XPAD 3.2 detector for a load of 41.6 N. b) Classical pattern resulting from the ψ integration of 0.2° as indicated by sectors in a).

Due to the texture the diffraction rings are incomplete and only sin²ψ segments have to be used (Figure 4a) for the stress analysis. Assuming plane-stress conditions and (111) fiber texture, the strain equation may be written for an equi-biaxial loading ($\sigma_{11}= \sigma_{22}$) as [9]:

$$\ln\left(\frac{1}{\sin\theta_{\psi}}\right) = 2\sigma_{22}\cdot\left[\frac{S_{11}-4S_{12}-S_{44}}{6}+\frac{S_{44}}{4}\right]\sin^2\psi + \ln\left(\frac{1}{\sin\theta^0}\right)$$

$$\sigma_{ii} = \sigma_{ii}^{R} + \sigma_{ii}^{A} \qquad \text{(eq. 1)}$$

where $\theta_\psi$ is the Bragg angle for a given $\psi$ (the superscript "0" denotes the stress-free Bragg angle) and, $\sigma_{11}$, $\sigma_{22}$ the macroscopic stresses in the thin film, $s_{11}$, $s_{12}$ and $s_{44}$ the elastic compliances. The superscript A (resp. R) is related to the applied (resp. residual) stress. The XRD total stresses can be calculated from $\ln(1/\sin\theta)$ versus $\sin^2\psi$ plots. Since tungsten is a locally elastically isotropic material, X-ray Elastic Constants are directly proportional to the macroscopic elastic constants E and $\nu$, and do not depend on grain interaction modelling [10-11]. This is the reason why the $\ln(1/\sin\theta)$ - $\sin^2\psi$ plots are linear. For Cu, a linear $\ln(1/\sin\theta)$ - $\sin^2\psi$ distribution is also assumed even if the film is locally anisotropic and textured. A small non-linear distribution has been reported in the case of ultra-thin film by Welzel et al [12]. This surface effect is neglected in the studied multilayers. Noteworthy, the crystallite group method referring to Eq.1 can be employed for weak textures [13], and can lead to a linear dependence of measured strain on $\sin^2\psi$ plots [14].

Figure 4b shows the $\ln(1/\sin\theta)$ - $\sin^2\psi$ plots for the (111) reflection of Cu and the (110) reflection of W measured for different sectors of 0.2° for the initial loading of the experiment (F11 = F22 = 19 N). The slopes of fitted lines are proportional to the in-plane stress (Eq. 1) in W and Cu sub-layers. Tungsten is in high compressive state, around -5 GPa while copper is approximately stress-free. The compressive stresses developed during film growth in ion beam sputtering processes are caused by atomic peening of the depositing film by the impact of high energy atoms [2].

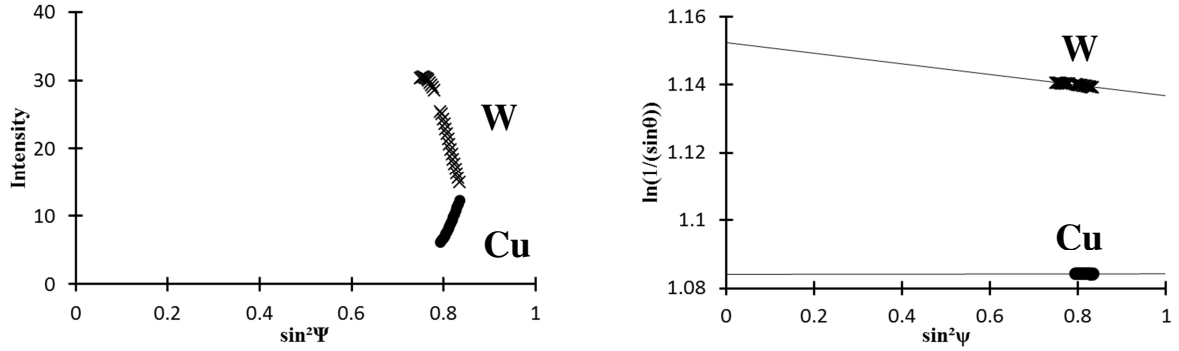


a) b)

Figure 4: Evolution of a) the diffraction peak intensity and b) $\ln(1/\sin\theta)$ distributions versus $\sin^2\psi$ at initial loading.

In a sake of clarity, figure 5 shows the $\ln(1/\sin\theta)$ - $\sin^2\psi$ plots and corresponding linear regressions only for a few increasing loading steps for W and Cu sublayers. The inserts show the evolution of the slope of the linear fits versus the applied load. These figures clearly reflect the change in the total stress (residual plus applied) for W and Cu during the tensile test (for both elastic and inelastic regimes). All the linear regressions in the elastic domain should cross at one point. As only a reduced $\sin^2\psi$ range is investigated, extrapolations lead to imprecision. However, it can be concluded that the remote 2D detection allows extracting with a sufficient accuracy the peak shifts and that the stress variations can be simultaneously monitored in both W and Cu phases. So, even with a very narrow-psi-range which leads to a relative uncertainty on total stress (residual plus applied) of about 30%, reliable stress variations (i.e. small applied stress increment) can be extracted. For W phase (Figure 5), the slope of the $\ln(1/\sin\theta)$-$\sin^2\psi$ linear regressions remains negative during the entire test. The total stress is first highly compressive (the residual stress value of the as-deposited W sublayers is about -5 GPa) and increases up to a still highly compressive stress state of approximately -3 GPa with the applied load. For Cu phase (Figure 5), the total stress is first nul and increases during the entire tensile test up to approximately +1.2 GPa. The slopes of the $\ln(1/\sin\theta)$ - $\sin^2\psi$ linear regression of the two phases increase linearly with the applied load and reach a plateau for an applied force of roughly 125 N. It is proposed that the applied stress plateau developed from a macroscopic applied strain of about 1% is caused by cracks initiation and propagation in the multilayer film. For uniaxial tensile test, cracks have been observed with different techniques: optical microscopy, scanning electron microscopy, atomic force microscopy or

indirectly by electrical measurements [16-18]. Generally, cracks are observed at relatively high applied strains (several %) and are difficult to observe in case of ductile metallic film onto polymers [16]. Recently, Djaziri et al. have also evidenced cracks at low strains in W/Cu nanocomposite film by extracting the yield stress surface [15]. Zhang et al. have shown that in Cu/Cr multilayer films (thickness of about 500 nm), the cracks appear first in Cr and then in Cu layers which are ductile, the rapidity of this effect being strongly dependent on the thickness period [19]. In the present study, the high compressive stress state of W sublayers combined with the high tensile stress state of Cu sublayers lead to an opposite scenario. Indeed, the cracks are expected either in Cu sublayers or at the W-Cu interfaces. Moreover, confined nanocrystalline Cu exhibits a small ductility compared to its coarse-grain counterpart and bears a large amount of tensile stress before failure [20].

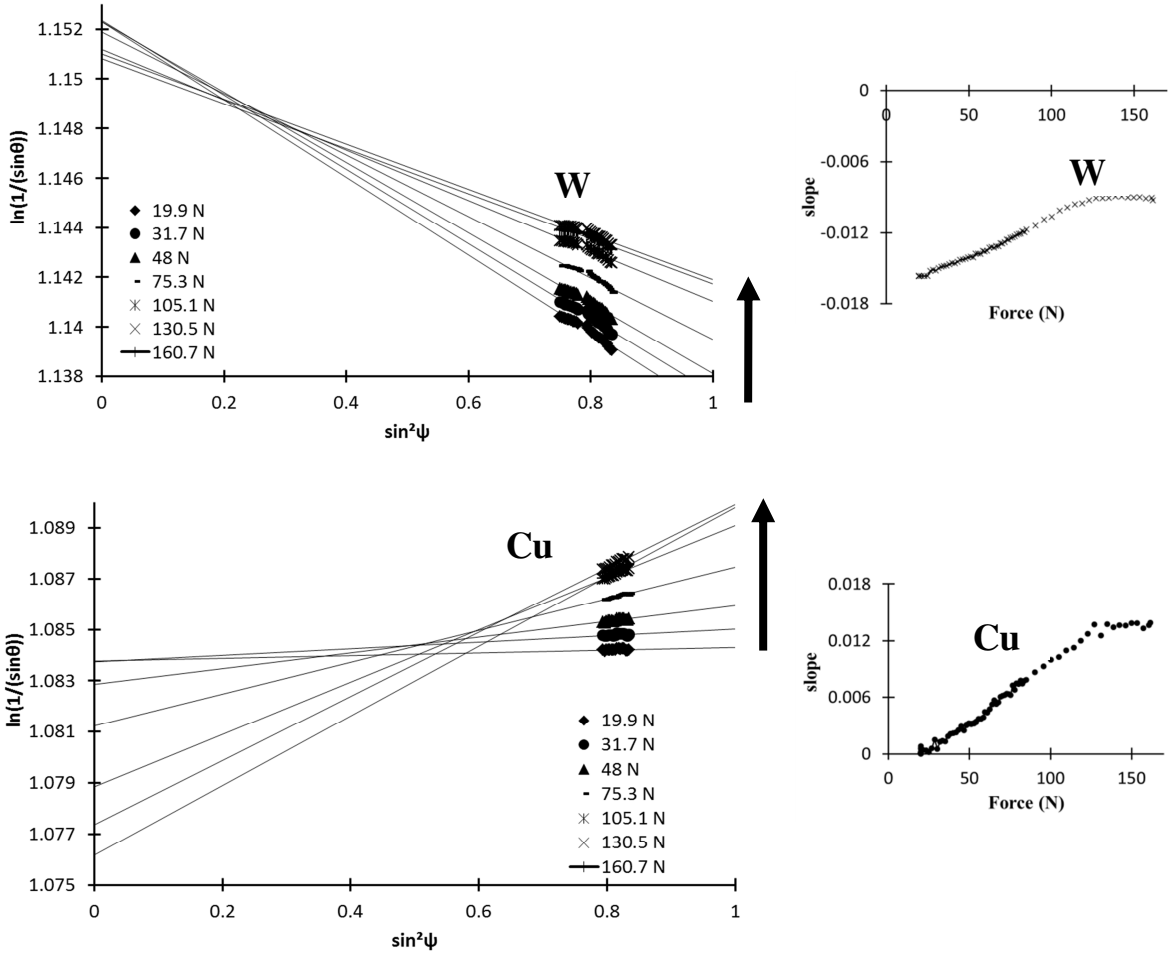


Figure 5: Evolution of ln(1/sinθ) - sin²ψ plots and associated linear regression with increasing loading steps. The inserts show the evolution of the slope of ln(1/sinθ) - sin²ψ plots as function of the applied force.

## Conclusion

In this paper, we demonstrate that 2D detector (XPAD 3.2) placed at a relatively large distance from the sample allows to monitor simultaneously W and Cu response during an in-situ continuous tensile test of a W/Cu multilayered thin film as thin as 150 nm. Diffraction peak position 2θ is extracted with accuracy for small ranges of ψ angles. This allow to study the evolution of the total stress (residual and applied) for W and Cu sublayers during the tensile test thanks to ln(1/sinθ) - sin²ψ plots. For W, total stress is highly compressive at the beginning of the test (residual stresses around -5 GPa) and becomes constant around -3 GPa at the end of the test. For Cu, total stress is first nil, becomes tensile during the test and saturates around +1.2 GPa. The stresses in the two

phases increase linearly with the applied load and reach a plateau at the same applied load revealing the presence of cracks. The failure is governed by the phase under tensile stress state (Cu) and not by the most brittle phase (W) contrary to what has been observed in similar multilayers [19]. The mechanical behavior is mainly governed by the residual stress state.

**References**

[1] Clyne, T. W., Withers, P. J., an Introduction to Metal Matrix Composites, Cambridge University Press, 1995.

[2] Hoffman, D. W., Thornton, J. A., Thin Solid Films, 40 (1977) 355-363.

[3] Kumar, K. S., Van Swygenhoven, H., Suresh, S., Acta Mater., 51 (2003) 5743–5774.

[4] Geandier, G., Thiaudière, D., Randriamazaoro, R. N., Chiron, R., Djaziri, S., Lamongie, B., Diot, Y., Le Bourhis, E., Renault, P. O., Goudeau, P., Bouaffad, A., Castelnau, O., Faurie, D., Hild, F., Rev. Sci. Instrum, 81(2010) 103903.

[5] Hild, F., Roux, S., Gras, R., Guerrero, N., Marante, M., Florez-Lopez, J., Opt Lasers Eng, 47 (2009) 495-503.

[6] Djaziri, S., Renault, P. O., Hild, F., Le Bourhis, E., Goudeau, P., Thiaudière, D., Faurie, D., J. Appl. Cryst., 44 (2011) 1071-1079.

[7] Le Bourlot, C., Landois, P., Djaziri, S., Renault, P. O., Le Bourhis, E., Goudeau, P., Pinault, M., Mayne-L'Hermite, M., Bacroix, B., Faurie, D., Castelnau, O., Launois, P., Rouzière, S., J. Appl. Cryst., 45 (2012) 38-47.

[8] Medjoubi, K., Bucaille, T., Hustache, S., Berar, J. F., Boudet, N., Clemens, J. C., Delpierre, P., Dinkespiler, B., J. Synchrotron Rad., 17 (2010) 486-495.

[9] Faurie, D., Renault, P. O., Le Bourhis, E., Goudeau, P., J. Appl. Phys., 98 (2005) 093511.

[10] Faurie, D., Castelnau, O., Brenner, R., Renault, P. O., Le Bourhis, E., Goudeau, P., J. Appl. Cryst., 42 (2009) 1073-1084.

[11] Hauk. V, Structural and Residual Stress Analysis by Nonedestructive Methods, Elsevier, 1997.

[12] Welzel, U., Kumar, Mittemeijer, Appl. Phys. Lett., 95 (2009) 111907.

[13] Gergaud. P, Labat. S, Thomas. O, Thin Solid Films, 319 (1998) 9-15.

[14] Pina. J, Dias. A, Francois. M, Lebrun. J. L., Surf. Coat. Technol. 96 (1997) 148-162.

[15] Djaziri, S., Faurie, D., Renault, P. O., Le Bourhis, E., Goudeau, P., Geandier, G., Thiaudière, D., Acta Mater., 61 (2013) 5067-5077.

[16] Cordill, M. J., Marx, V. M., Phil. Mag. Lett., 93 (2013) 618-624.

[17] Leterrier, Y., Prog. Mater. Sci, 48 (2003) 1.

[18] Roland, T., Arscott, S., Sabatier, L., Buchaillot, L., Charkaluk, E., J. Micromechanics Microengineering, 21 (2011) 125005.

[19] Zhang, J. Y., Zhang, X., Liu, G., Zhang, G.J., Sun, J., Scripta Mater., 63 (2010) 101-104.

[20] Champion, Y., Langlois, S., Guerin-Mailly, P., Bonnentien, J. L., Hÿtch, M. J., Science, 300 (2003) 310.